COBEM 2023 27TH INTERNATIONAL CONGRESS OF MECHANICAL ENGENEERING

ABCM Brazilian Society of Mechanical Sciences and Engineering
27th ABCM International Congress of Mechanical Engineering
December 04-08, 2023, Florianópolis-SC, Brazil

COB-2023-1538
Validation of a simulation model to predict the drag on cylinders in different tandem arrangements

Pedro Corrêa Dallabrida
Filipe Dutra da Silva
TEG - Thermofluids Engineering Group, Federal University of Santa Catarina, Joinville-SC, 89219-600, Brazil
pedro.dallabrida@teg.ufsc.br, filipe.dutra@teg.ufsc.br

Abstract. *This work aims to achieve a low computational cost mesh with reliable results on the drag for a tandem cylinder case. Varying one parameter at a time for proper comparison, the influence of the average y+ value along both cylinders was considered, as well as the importance of the total thickness of the prismatic cells layers was analyzed. The refinement of the mesh on its depth was also evaluated. Finally, a global refining test was performed using the grid convergence index criteria for evaluating grid convergence. For validation purposes, the results obtained by the meshes were compared with experimental data found in the literature for a turbulent flow with Reynolds number Re = 1.66 x 10^5 and cylinders with diameters D = 0.05715 m. Two cases were analyzed, one in which the center-to-center distance between the cylinders was L = 3.7D and other in which L=1.435D. In both cases, results for the first cylinder were in good agreement with the experimental data. For the second cylinder, however, due to limitations of the modeling, a greater deviation was found.*

Keywords: *Tandem cylinders, CFD simulation using OpenFOAM.*

1. INTRODUCTION

Flow over tandem cylinders is a recurrent case studied in engineering due to its application in several areas. This problem can be found in aeronautical engineering, e.g. in landing gear, and in naval engineering, e.g in offshore oil platforms and wind turbines. Thus, given its high applicability and complexity, studies seeking to characterize this flow were carried out.

In a wind tunnel experiment made by Alam and Meyer (2011), six different interaction mechanisms were observed for different distances between cylinders, angle of attack of the upcoming flow and Strouhal number: boundary layer and cylinder interaction, shear layer and cylinder interaction, shear layer and shear layer interaction, vortex and cylinder interaction, vortex and shear layer interaction, and vortex and vortex interaction. For each of the listed mechanisms, the fluctuating induced forces behavior was distinct. It was concluded that vortex and shear layer interactions intensifies aerodynamics/hydrodynamics forces, and wake and cylinder interaction reduces forces and the unsteadiness of the flow.

Zdravkovich (1985) sought to describe the flow-field in tandem cylinders relating the distance L between the centers of the cylinders. For distances $L < 1.1D$, the bodies behave as a single slender body and vortex shedding occurred only downstream of the rear cylinder. For a distance of $1.1D < L < 1.6D$, oscillations in the reattachment of the shear layers occur in the frontal region of the rear cylinder. For $1.6D < L < 2.4D$, the reseeding of the shear layers on the rear cylinder occurs in a quasi-steady manner. For $2.4D < L < 3.2D$, occasional vortex appear in the regions between the cylinders. Between $3.2D$ and $3.8D$, these vortex shedding occurs almost continuously. For values above $3.8D$ the cylinders do not interact with each other and can be seen as independent.

A series of studies were carried out at the NASA Langley Research Center seeking to characterize the case of tandem cylinders for a Reynolds of $Re = 1.66 \times 10^5$. Jenkins *et al.* (2005) carried out tests in the Basic Aerodynamic Research Tunnel (BART) and characterized the pressures along the surfaces of the two cylinders as well as the velocity profiles, using transition strips on the front cylinder to guarantee a turbulent boundary layer. In later work, Jenkins *et al.* (2006) used the same experimental setups characterizing surface flow using steady and unsteady pressure measurements and surface flow visualization. Neuhart *et al.* (2009) performed new measurements on BART, adding more information to the database of this experiment.

Khorrami *et al.* (2007) tried to replicate numerically the work of Jenkins *et al.* (2005) using a compressible Unsteady Reynolds Averaged Navier Stokes (URANS) in the CFL3D modeling code in a 2D grid with 3.19×10^5 points. Doolan (2009) developed a numerical model in OpenFOAM using incompressible URANS with turbulence model SST $k - \epsilon$, calculating results in the aerodynamic and acoustic fields.

Lockard *et al.* (2007) used the same tandem cylinders setup to study the noise generated for these cases in the Quiet Flow Facility (QFF). Brès *et al.* (2012) approached the problem three-dimensionally, seeking to faithfully recreate numerically the experiment carried out in the QFF, calculating the aerodynamic field through the Lattice Boltzmann method.

Weinmann *et al.* (2014) simulated tandem cylinders for flow and noise predictions in a relatively coarse grid using a RANS/LES hybrid approach called modified Flow Simulation Methodology (FSM) introduced by (Speziale, 1998). It was used with $k-\omega$-SST (FSM-SST) and Explicit-Algebraic-Stress-Model (FSM-EASM) and results were compared with SAS and IDDES approaches. It was found that the flow around the tandem cylinder configuration is very sensitive to the used turbulence model, in which the FSM-SST provided better flow field and acoustics agreement when compared to the reference data.

Sainte-Rose *et al.* (2014) compared the results of numerical simulations for the BART tandem cylinders experiment between two different turbulence models, a LES Variational Multi-Scale (VMS) and a classic LES method. The domain was three dimensional and measured only $4D$ in the spanwise direction. Results showed that LES-VSM predicted better the separation point and the turbulent kinetic energy, especially in the gap region. The drag coefficient for both turbulence models were, however, were slightly overpredicted for both cylinders.

Therefore, the present work proposes to investigate the parameters that influence the accuracy of a mesh, aiming to combine low computational cost and reliability.

2. METHODOLOGY

To generate a mesh with low computational cost and with good agreement with the experimental data, a series of investigations about the parameters that influence the most the results was conducted. This section aims to provide details about the different meshes generated.

2.1 Geometry

The initial geometry was based on the computational domain used by Batista (2022), who studied the sensitivity of local refinements in a mesh that tried to replicate the experiment by Jenkins *et al.* (2005), and by Chadlvski and Dutra da Silva (2021), who studied the same case looking to predict the aerodynamic noise numerically. The computational domain is a three-dimensional rectangular box with the inlet located at x = -13D and the outlet located at x = 35D. As investigated by Batista (2022), the mesh size in its spanwise direction is not so relevant for the aerodynamic coefficients and it was set to just $4D$. The local refinements remained the same as used by Batista (2022). The center of the front cylinder is located at $x = 0$ and $y = 0$, while the center of the rear cylinder is a parametric variable. The computational domain is depicted in Fig. 1.

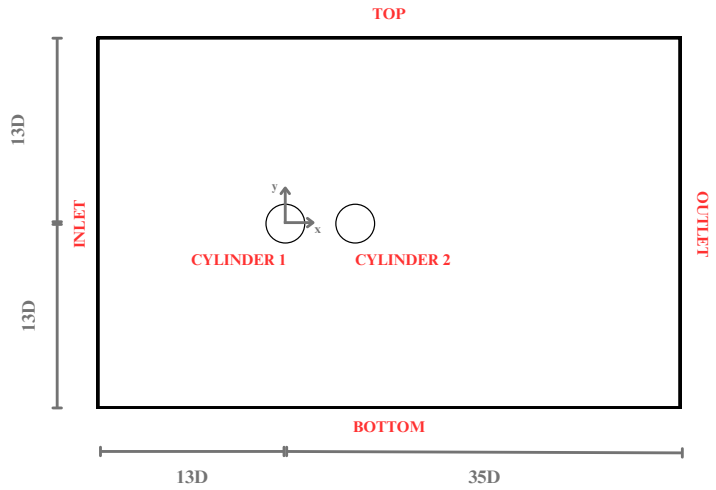

Figure 1: Computational domain in the xy-plane and boundary conditions.

All geometries and meshes were generated using snappyHexMesh, which is mesh generator code inside OpenFOAM. Figure 2 shows the cylinders and mesh refinement regions in more detail.

The diameter of the cylinders is D = 0.05715 m and the freestream velocity is U = 44 m/s, resulting in a Reynolds number $Re = 1.66 \times 10^5$. A series of comparisons was conducted for the case in which the distance between the cylinders centers was set to L = 3.7D. For validation, all curves results were compared with the experimental data extracted from the case of Jenkins *et al.* (2005) and the drag coefficients C_d were compared to data extracted from Jenkins *et al.* (2006) and Neuhart *et al.* (2009). Finally, a case with L = 1.435D was simulated and also compared.

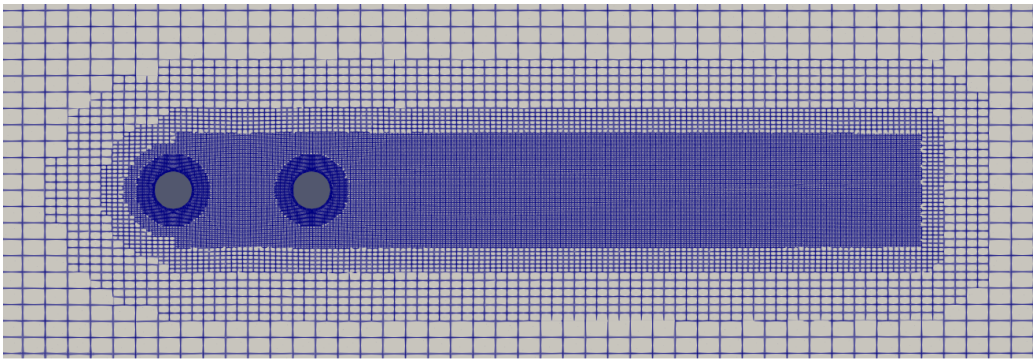

Figure 2: View from the xy-plane of the mesh refinement regions.

2.1.1 Influence of y+ value

The first analysis was about the influence of y+ value while the overall thickness of the prismatic cells was set to a fixed value. Thus, for a thickness of $0.043D$, the results of three meshes with different average y+ values were compared. Table 1 shows the values of each mesh for both cylinders.

Table 1: Number of cells, mean and max y+ value for each cylinder and overall thickness of the prismatic cells

Number of cells	Mean y+ front cyl	Mean y+ rear cyl	Max y+ front cyl	Max y+ rear cyl	Thickness
3902522	0.9243	0.8277	1.7210	1.4834	$0.043D$
3676558	1.9405	1.7572	3.8161	3.4128	$0.043D$
3496190	3.6771	3.3742	7.3637	6.6627	$0.043D$

2.1.2 Influence of the layers overall thickness

The response to the change in the total thickness of the prismatic layers was also evaluated. An initial size of the cell adjacent to the wall and a geometric ratio of layer growth were defined, varying the thickness based on the change in the number of layers. Thus, for a fixed expansion rate of 1.15 and a fixed first cell size of 11.6 μm, guaranteeing y+ < 1 and similar between the meshes, a variation of 33% of the total thickness was established, both up and down. This variation, however, could not be achieved exactly due to the way the layers are generated. Table 2 shows the value of the total thickness and y+ for each of the meshes.

Table 2: Number of cells, mean max y+ value for each cylinder and overall thickness of the prismatic cells

Number of cells	Mean y+ front cyl	Mean y+ rear cyl	Max y+ rear cyl	Max y+ rear cyl	Thickness
3765559	0.9211	0.8313	1.7043	1.4928	$0.027D$
3902522	0.9243	0.8277	1.7210	1.4834	$0.043D$
3991159	0.9407	0.8228	1.7344	1.4828	$0.057D$

2.1.3 Influence of the refinement in spanwise direction

The influence of the refinement on the spanwise direction was verified. The objective is to verify if a less refined mesh in this direction would not significantly alter fluid dynamic coefficients, in addition to reducing the computational cost of the simulation. The results were compared when changing the number of blocks from 240 to 160 and 80. The same prismatic layer thickness and first cell height were used, ensuring the same y+ values. The data for each mesh is shown in Tab. 3.

Table 3: Number of cells, thickness of the prismatic layer and number of blocks in spanwise direction along cylinders

Number of cells	Thickness of prismatic cells	Number of blocks in spanwise direction
3991159	$0.057D$	240
2702376	$0.057D$	160
1353925	$0.057D$	80

2.1.4 Global refinement

After all the analyses, the effect of the global mesh refinement was evaluated using the grid convergence index (GCI) (Roache, 1997; Celik *et al.*, 2008). Thus, based on a global refining ratio value of r = 1.3, three meshes were compared, the one obtained after analysing all previous parameters, one coarser and one more refined. The r values were not exact and are shown, as well as the number of cells for each mesh, in Table 4.

Table 4: Number of cells, mean and max y+ value and convergence ratio r for GCI analysis

Meshes	**Number of cells**	**Mean and max y+ front cyl**	**Mean and max y+ rear cyl**	r
Coarser	479921	1.8787; 3.7468	1.8772; 3.4399	1.41
Intermediate	1353925	0.9243; 1.7210	0.8277; 1.4834	-
Finer	3229674	0.1996; 0.3792	0.17563; 0.3239	1.33

2.1.5 Effects of varying distance between cylinders

Finally, a simulation with a different distance between the cylinders center was performed, changing the distance from $3.7D$ to $1.435D$. The mesh used has the same characteristics as the intermediate mesh used in GCI analysis. The result computed for the drag coefficient values was compared with data found in the work by Jenkins *et al.* (2006) and Neuhart *et al.* (2009) while pressure coefficients distribution along the cylinder were compared with the experimental data of Jenkins *et al.* (2005). This stage of the work seeks to validate the values adopted in each of the previous parameters investigations for a different L value.

2.2 Simulation Model

The cases were simulated in OpenFOAM v2212 using incompressible Unsteady Reynolds Averaged Navier Stokes and SST k-ω turbulence model (Menter, 1994). A Multi-directional cell-limited scheme was adopted for the gradient terms and for the advective terms a second order linear upwind scheme was used. The Pressure-Implicit with Splitting of Operators (PISO) algorithm was used.

On the inlet, top and bottom boundaries, a free-stream velocity condition with a free-stream gauge pressure of 0 Pa was imposed. For the outlet, a fixed gauge pressure of 0 Pa was prescribed with a zero-gradient condition for velocity. No-slip wall condition was used on the cylinder surfaces. The turbulence variables k and ω were calculated based on a turbulence intensity I = 0.1% and turbulent cinematic viscosity ratio ν_t/ν = 1.

Time step used was tU_∞/D = 0.003849, guaranteeing a maximum Courant number < 1. All simulations were conducted until the mean and standard deviation of the drag coefficient computed on both cylinders did not show a variation greater than 1% over time. From that point on, the simulation was considered to have reached an statistically stationary condition. For a simulation started without interpolation of the velocity and pressure fields, it was found that 0.35 seconds of simulation time represented the initial transient, and should be discarded. About 30000 time steps were used to calculate the averages.

3. RESULTS AND DISCUSSION

In this section, the results for each analysis described in the methodology are presented. Variations of the results are discussed in terms of of average drag coefficient, pressure coefficient measured in the middle of the cylinder and wake velocity profiles.

3.1 Influence of y+ value

The computational mesh with an y+ < 1 was set as benchmark for comparison and two others geometries were simulated with y+ > 1 and y+ > 3. All geometries shared $0.043D$ as the total thickness of the prismatic cells. Figure 3 presents the pressure coefficient on the front cylinder surface (Fig. 3a) and rear cylinder surface (Fig. 3b). The position on the surface is measured clockwise from the stagnation point. Results were extracted from the simulations up to 180º, assuming symmetry. It is possible to note that, in the upstream cylinder, the pressure coefficient for all meshes are similar between 0º and 60º. For 100º < θ < 180º, the front cylinder wake region, the mesh with y+ < 1 has higher pressure coefficients and is closer to the experimental data extracted from Jenkins *et al.* (2005). For the rear cylinder, between 120º and 180º the pressure coefficient is underestimated for all meshes, but again, the mesh with y+ < 1 is closer to the experimental data. Similar behavior is found for the second cylinder. It is noticeable that, as y+ decreases, results get closer to the experimental data, as expected due a better description of the boundary layer behavior close to the wall with y+ < 1.

As a consequence, the mean drag coefficients are better calculated by the mesh with y+ < 1, as shown in Tab. 5, given that from Neuhart *et al.* (2009), mean drag coefficient for the upstream cylinder is 0.6456 and 0.3172 for the downstream

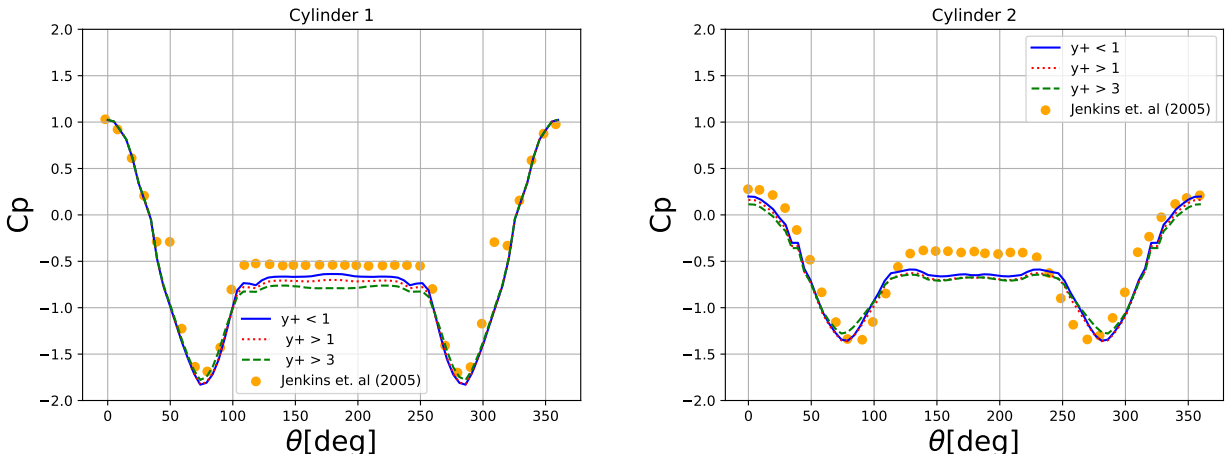

(a) Front cylinder.

(b) Rear cylinder.

Figure 3: Pressure coefficient on the surface of both cylinders comparing numerical results for different y+ values to experimental data extracted from Jenkins *et al.* (2005)

cylinder. The mesh with y+ < 1 deviates 3.38% from experimental data for the upstream cylinder and mesh with y+ > 1 deviates 4.26%. However, as y+ increases, results for the downstream cylinder tends to approximate to experimental data. Nonetheless, adopting a mesh with lower resolution because it is more in line with experimental results would characterize overfitting, given that the numerical error would be adjusted according to a desired result.

Table 5: Mean drag coefficients for each cylinder for different mean y+ values

Mean y+ value	C_d **cyl 1**	C_d **cyl 2**	**Cyl 1 deviaton**	**Cyl 2 deviation**
y+ < 1	0.6280	0.3968	-	-
y+ > 1	0.6777	0.3888	7.91%	2.02%
y+ > 3	0.7523	0.3813	19.79%	3.91%

Thus, although a lower y+ implies more computational cost, it is not significantly greater to justify the use of a mesh with y+ > 1 as the results tend to be inaccurate.

3.2 Influence of layers overall thickness

The purpose of this subsection is to evaluate how changing prismatic cell layer overall thickness affects pressure coefficient and drag results. The mesh obtained by the previous analysis was used as a baseline, and two meshes, one with higher and one with lower thickness were simulated. Figure 4 shows the pressure coefficient on the front cylinder surface (Fig. 4a) and rear cylinder surface (Fig.4b) for each mesh. The behaviour of the pressure coefficient curves are very similar to the ones already presented. It is difficult to see any tendency occurring in Fig. 4a, but in Fig.4b it is possible to see how the mesh with $0.027D$ deviates from the others and from the experimental data. However, the other two meshes present very similar behavior by looking only at pressure coefficient curves.

Table 6 shows mean drag coefficients calculated for each cylinder. It is important to have in mind, that from Neuhart *et al.* (2009), the drag coefficient for the upstream cylinder is 0.6456 and for the downstream cylinder is 0.3172. Clearly, results shown in Tab. 6 points to a better agreement with experimental data for both cylinders for the mesh with higher prismatic cells thickness.

Table 6: Mean drag coefficients for each cylinder for different thicknesses of prismatic cell layers

Layers thickness	C_d **cyl 1**	C_d **cyl 2**	**Cyl 1 deviaton**	**Cyl 2 deviation**
$0.043D$	0.6280	0.3968	-	-
$0.057D$	0.6421	0.3804	2.24%	4.13%
$0.027D$	0.6058	0.4301	3.54%	8.40%

Due to the deviations of numerical results compared with experimental data for the rear cylinder, a new mesh was generated increasing by 33% the thickness of the prismatic cells for the downstream cylinder. However the results did

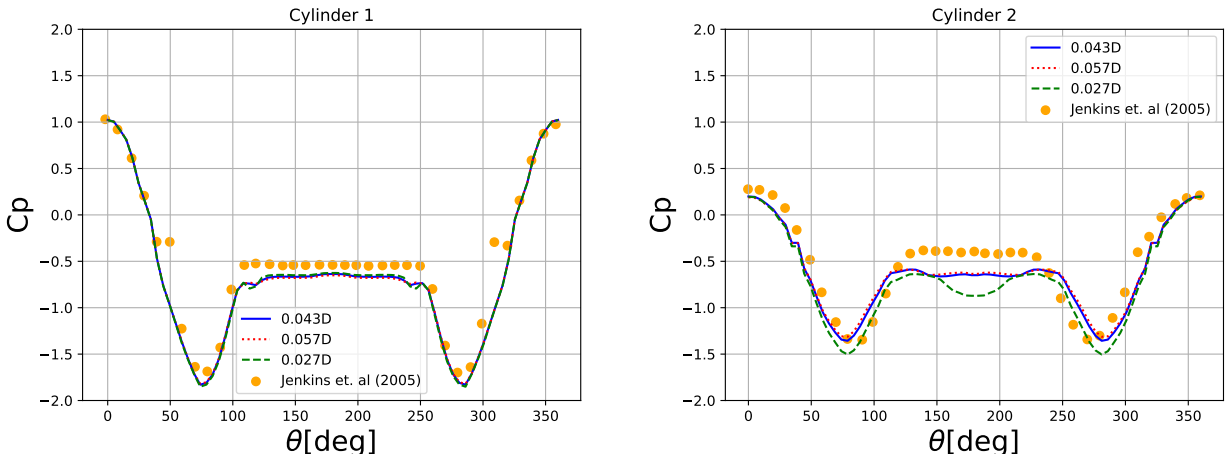

(a) Front cylinder.

(b) Rear cylinder.

Figure 4: Pressure coefficient on the surface of both cylinders comparing numerical results for different thicknesses of prismatic cell layers to experimental data extracted from Jenkins *et al.* (2005)

not show significant improvements. Based on this analysis, we concluded that the mesh with $0.057D$ thickness for the prismatic cells for both cylinders was more accurate and with no relevant increase in the computational cost, as the cell number did not increase significantly.

3.3 Influence of the refinement in the spanwise direction

The sensitivity of the results were checked to different refinements in spanwise direction. It was hypothesized that the baseline mesh was excessively refined in this direction along both cylinders and that it was causing unnecessary increase in computational cost, so two other coarser meshes were tested. Figure 5 shows the pressure coefficient curves for each mesh with different volumes in the spanwise direction along both cylinders. It is not possible to notice significant differences between each mesh. Table 7 shows the mean drag coefficient for three meshes. The results are not greatly impacted as the

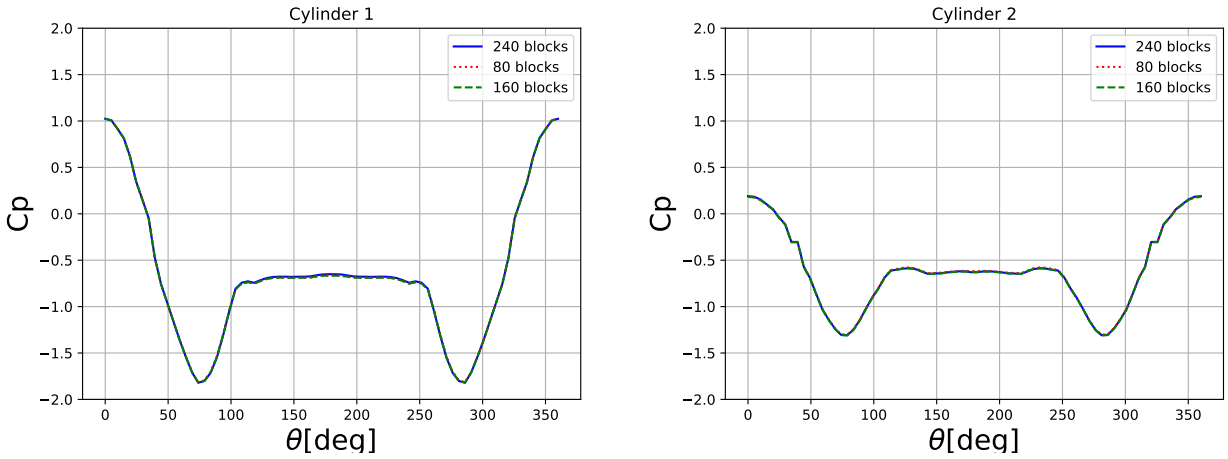

(a) Front cylinder.

(b) Rear cylinder.

Figure 5: Pressure coefficient on the surface of both cylinders comparing numerical results from meshes with different refinement in spanwise direction

values differentiate only by 1.74% on the front cylinder and 0.22% for the rear cylinder.

Therefore, given the considerable reduction in computational cost (number of cells reduced from 3991159 to 1353925) and the minimal impact in the fluid dynamic coefficients, the mesh with 80 blocks in the spanwise direction was adopted for the next analysis.

Table 7: Mean drag coefficients for each cylinder calculated from meshes with different refinement in spanwise direction along cylinders

Number of blocks	C_d **cyl 1**	C_d **cyl 2**	**Cyl 1 deviaton**	**Cyl 2 deviation**
240	0.6421	0.3804	-	-
160	0.6518	0.3765	1.51%	1.03%
80	0.6532	0.3796	1.74%	0.22%

3.4 Global refinement

Finally, a global refinement analysis was performed based on the grid convergence index. Figure 6 shows the pressure coefficient for each mesh. In Fig. 6a, for the upstream cylinder, very similar results can be observed between the intermediate and finer mesh. However, the coarse mesh differs from the others underpredicting the pressure coefficient, especially in the wake region, between 100º and 180º. The same pattern can be seen for the second cylinder in Fig. 6b, although the values predicted by the finer mesh are slightly below the intermediate mesh between 100º and 180º.

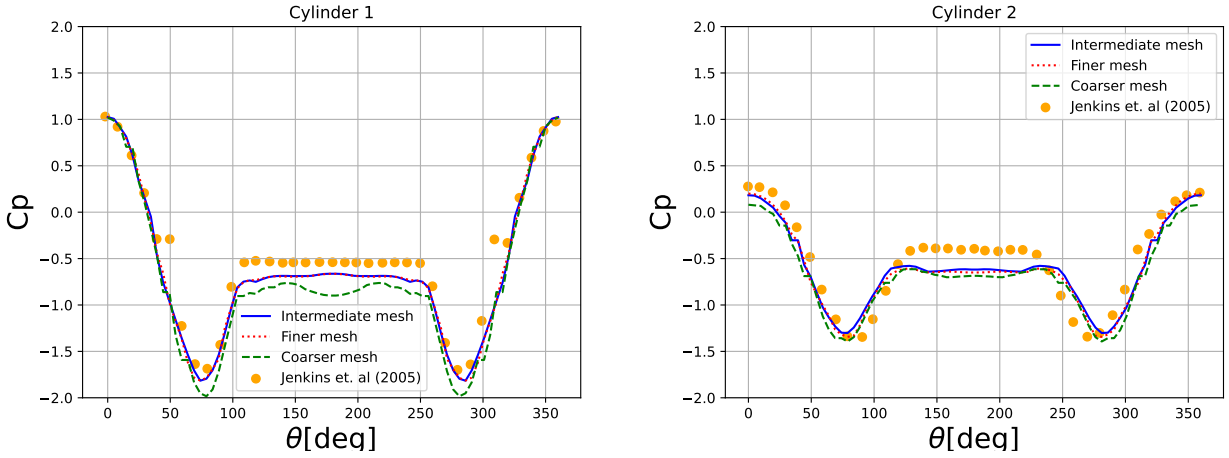

(a) Front cylinder.

(b) Rear cylinder.

Figure 6: Pressure coefficient on the surface of both cylinders comparing numerical results from meshes with different global refinement to experimental data extracted from Jenkins *et al.* (2005)

The streamwise velocity between both cylinders along the centerline is shown in Fig. 7 Again, results from the coarsest mesh show the highest deviations from the experimental data extracted from BART presented by Lockard *et al.* (2007). The fine and intermediate meshes have very similar behavior. All the simulations overpredicted the velocity magnitudes and failed to capture the peak positions.

Table 8 shows the mean drag coefficient results for each mesh. The difference between the results from the intermediate mesh and finer mesh are not significant, especially for the upstream cylinder, in which the difference is only 0.28% for the first cylinder and 3.28% for the second. Applying GCI method, the extrapolated drag found is 0.6504 for the upstream cylinder and 0.3912 for the downstream. Furthermore, the results of the method indicate a reduction of the influence of refining on the results. Therefore, the intermediate mesh proved to be able to calculate the fluid dynamic coefficients satisfactorily, and a refinement of this magnitude does not seem to be an advantageous choice, since the computational cost increases significantly.

Table 8: Mean drag coefficients for each cylinder calculated from meshes with different global refinement

Meshes	C_d **cyl 1**	C_d **cyl 2**	**Cyl 1 deviaton**	**Cyl 2 deviation**
Intermediate mesh	0.6518	0.3765	-	-
Finer mesh	0.6507	0.3888	0.18%	3.28%
Coarser mesh	0.7491	0.2869	14.93%	23.80%

The intermediate mesh is, then, compared to measurements available in literature. To a proper comparison, drag coefficient is calculated the same way as in the work by Jenkins *et al.* (2006) (where measurements were made at BART facilities) and Neuhart *et al.* (2009), in which the drag is taken from the integration of the pressure coefficient curve in the

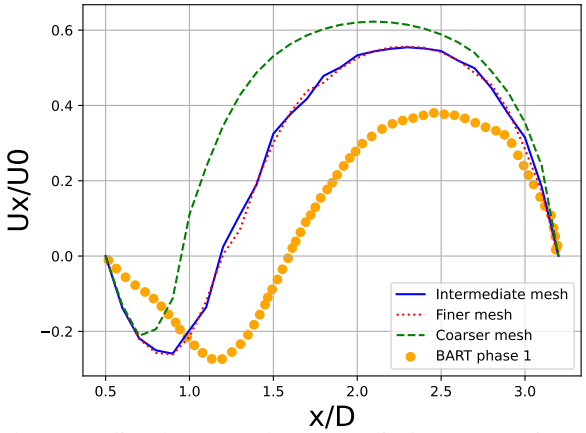

Figure 7: Velocity profile on the centerline between the two cylinders comparing numerical results from meshes with different global refinement to experimental data from BART.

middle of the cylinder (resulting in drag coefficient per unit span).

Table 9: Comparison between numerical drag coefficients per unit span calculated from pressure coefficient curve integration and measurements found in literature for $L = 3.7D$

Case	C_d **cyl 1**	C_d **cyl 2**	**Cyl 1 deviaton**	**Cyl 2 deviation**
Current numerical	0.6656	0.3397	-	-
BART (phase 1)	0.6015	0.2963	10.65%	14.65%
BART (phase 2)	0.6328	0.3172	5.19%	7.08%
Neuhart *et al.* (2009)	0.6456	0.3172	3.10%	7.08%

It is noticeable that when compared with the experimental values, the drag on the rear cylinder is overestimated. This can be justified by the poor prediction of streamwise velocity in the wake in the front cylinder.

3.5 Effects of varying the distance between cylinders

The mean pressure coefficient curves for the case with $L = 1.435D$ are shown in Figure 8. The upstream cylinder (Fig. 8a) presents good agreement compared to measurements from wind tunnel, with the numerical curve following very closely the experimental data, except for between 250 and 300 degrees, interval that represents the boundary layer detachment at the bottom of the cylinder, where the simulation fails replicate the empirical behavior.

In Fig.8b, it is shown the pressure coefficient for the downstream cylinder. Notice that both in the simulations and experiments, especially in the measurements by Jenkins *et al.* (2005), the curve is asymmetric, an odd result. In the wind tunnel that could be explained by a slight misalignment between the cylinders, hypothesis that was confirmed by the work of Khorrami *et al.* (2007). It was verified that for $L = 1.435D$, an angle of attack of only 1 degree could cause such asymmetric results. In the simulation, however, this could not happen, since there cannot be a misalignment between the cylinders. One hypothesis is that some asymmetry in the mesh generated by snappyHexMesh was inducing this results, but that could not be checked by the authors.

Nonetheless, despite the inaccuracy in the pressure coefficient distribution, especially in the downstream cylinder, results for the drag coefficient, calculated by OpenFOAM's post-processing module, are presented in Tab.10 and show good agreement with empirical data.

Table 10: Mean drag coefficients calculated by OpenFOAM's function for each cylinder for the case with $L = 1.435D$ comparing numerical results to experimental data found in literature

Cases	C_d **cyl 1**	C_d **cyl 2**	**Cyl 1 deviaton**	**Cyl 2 deviation**
$1.435D$	0.6505	-0.1726	-	-
BART (phase 1)	0.5954	-0.1718	9.25%	0.47%
BART (phase 2)	0.6255	-0.1743	4.00%	0.98%
Neuhart *et al.* (2009)	0.6359	-0.1923	2.30%	10.24%

However, when the same integration procedure of the pressure coefficient is done - resulting in drag per unit span -

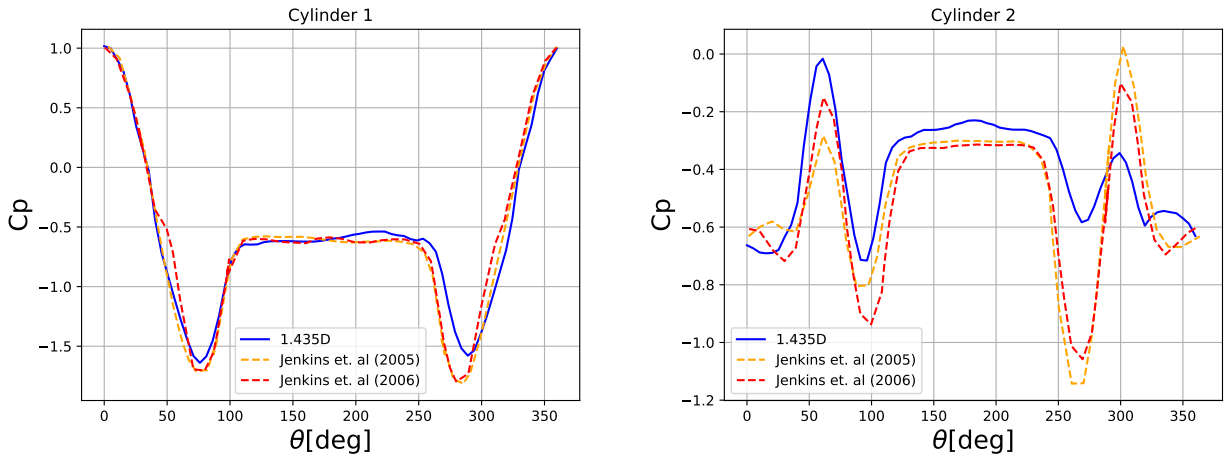

(a) Front cylinder.

(b) Rear cylinder.

Figure 8: Pressure coefficient on the surface of both cylinders for $L = 1.435D$ comparing numerical results to Jenkins *et al.* (2005) and Jenkins *et al.* (2006) experimental data.

the drag for the downstream cylinder deviates significantly from the experimental, result that arises from the discrepancy of the pressure coefficient curves. For the front cylinder, nonetheless, drag approaches experimental data, except when compared to Neuhart *et al.* (2009). These results are shown in Tab. 11.

Table 11: Mean drag coefficients per unit span calculated from pressure coefficient curve integration for each cylinder. Case with $L = 1.435D$ comparing numerical results to experimental data found in literature

Cases	C_d **cyl 1**	C_d **cyl 2**	**Cyl 1 deviaton**	**Cyl 2 deviation**
$1.435D$	0.6089	-0.3921	-	-
BART (phase 1)	0.5954	-0.1718	2.27%	128.23%
BART (phase 2)	0.6255	-0.1743	2.65%	124.96%
Neuhart *et al.* (2009)	0.6359	-0.1923	4.25%	103.90%

4. CONCLUSION

We have performed local and global grid sensitivity studies and validated a numerical setup to predict the flow field around tandem cylinders. Good agreement with the experimental data was achieved for the coefficients of the upstream cylinder, but the results tend to deviate more for the downstream cylinder. This could be explained by the chosen turbulence model. Since the nature of the flow in tandem cylinders is essentially unsteady, URANS simulations are not capable of capturing the total problem complexity. Therefore, since the physics on the downstream cylinder is greatly influenced by the upstream cylinder vortices wake, this could justify the downstream fluid dynamic coefficients deviation compared to experimental data. Better results should be expected to be found by different turbulence models, such as Large Eddy Simulations or other hybrid methods. Those are, however, computationally costly compared to URANS and do not fit the scope of this work.

Furthermore, from the results shown, it can be said that the attempt to generalize a mesh capable of reliably predicting drag for different cases of tandem cylinders was failed. The difficulty of this objective lies in the fact that the dynamics of the flow around the cylinders changes depending on the distance between them, and for a better prediction of the fluid dynamic coefficients, individual analyzes of mesh parameters relevant to each case should offer better results.

5. ACKNOWLEDGEMENTS

All simulations were only able to be conducted thanks to the computational resources provided by Laboratório de Computação Científica (LCC) at Universidade Federal de Santa Catarina (UFSC).

6. REFERENCES

Alam, M.M. and Meyer, J.P., 2011. "Two interacting cylinders in cross flow". In *Physical Review E - Statistical, Nonlinear, and Soft Matter Physics*. Vol. 84. ISSN 15393755. doi:10.1103/PhysRevE.84.056304.

Batista, P.A., 2022. "Algorithm for automating mesh generation and simulation of flow around tandem cylinders using open source tools (in portuguese)". In *Undergraduate Program in Aerospace Engineering, Federal University of Santa Catarina*. Joinville, Brasil.

Brès, G.A., Freed, D., Wessels, M., Noelting, S. and Pérot, F., 2012. "Flow and noise predictions for the tandem cylinder aeroacoustic benchmark". In *Physics of Fluids*. Vol. 24. ISSN 10706631. doi:10.1063/1.3685102.

Celik, I., Ghia, U., Roache, P., Freitas, C., Coloman, H. and Raad, P., 2008. "Procedure for Estimation and Reporting of Uncertainty Due to Discretization in CFD Applications". *Journal of Fluids Engineering*, Vol. 130, No. 7. ISSN 0098-2202. doi:10.1115/1.2960953. 078001.

Chadlvski, J. and Dutra da Silva, F., 2021. "Prediction of aerodynamic noise generated by cylinders in uniform flow using openfoam". In *Proceedings of the 26th International Congress of Mechanical Engineering - COBEM 2021*. doi:10.26678/ABCM.COBEM2021.COB2021-1128.

Doolan, C.J., 2009. "Flow and noise simulation of the nasa tandem cylinder experiment using openfoam". In *15th AIAA/CEAS Aeroacoustics Conference (30th AIAA Aeroacoustics Conference)*. doi:10.2514/6.2009-3157.

Jenkins, L.N., Khorrami, M.R., Choudhari, M.M. and McGinley, C.B., 2005. "Characterization of unsteady flow structures around tandem cylinders for component interaction studies in airframe noise". In *Collection of Technical Papers - 11th AIAA/CEAS Aeroacoustics Conference*. Vol. 1. doi:10.2514/6.2005-2812.

Jenkins, L.N., Neuhart, D.H., McGinley, C.B., Choudhari, M.M. and Khorrami, M.R., 2006. "Measurements of unsteady wake interference between tandem cylinders". In *Collection of Technical Papers - 36th AIAA Fluid Dynamics Conference*. Vol. 1. doi:10.2514/6.2006-3202.

Khorrami, M.R., Choudhari, M.M., Lockard, D.P., Jenkins, L.N. and McGinley, C.B., 2007. "Unsteady flowfield around tandem cylinders as prototype component interaction in airframe noise". *AIAA Journal*, Vol. 45. ISSN 00011452. doi:10.2514/1.23690.

Lockard, D.P., Khorrami, M.R., Choudhari, M.M., Hutcheson, F.V., Brooks, T.F. and Stead, D.J., 2007. "Tandem cylinder noise predictions". In *13th AIAA/CEAS Aeroacoustics Conference (28th AIAA Aeroacoustics Conference)*. doi:10.2514/6.2007-3450.

Menter, F.R., 1994. "Two-equation eddy-viscosity turbulence models for engineering applications". *AIAA Journal*, Vol. 32. ISSN 00011452. doi:10.2514/3.12149.

Neuhart, D.H., Jenkins, L.N., Choudhari, M.M. and Khorrami, M.R., 2009. "Measurements of the flowfield interaction between tandem cylinders". In *15th AIAA/CEAS Aeroacoustics Conference (30th AIAA Aeroacoustics Conference)*. doi:10.2514/6.2009-3275.

Roache, P.J., 1997. "Quantification of uncertainty in computational fluid dynamics". *Annual Review of Fluid Mechanics*, Vol. 29, No. 1, pp. 123–160. doi:10.1146/annurev.fluid.29.1.123.

Sainte-Rose, B., Leca, C., Allain, O. and Dervieux, A., 2014. "A study of les models for the simulation of a turbulent flow around supercritical tandem cylinders". In *Proceedings of the International Conference on Offshore Mechanics and Arctic Engineering - OMAE*. Vol. 2. doi:10.1115/OMAE2014-24031.

Speziale, C.G., 1998. "A combined large-eddy simulation and time-dependent rans capability for high-speed compressible flows". *Journal of Scientific Computing*, Vol. 13. ISSN 08857474. doi:10.1023/A:1023266932231.

Weinmann, M., Sandberg, R.D. and Doolan, C., 2014. "Tandem cylinder flow and noise predictions using a hybrid rans/les approach". *International Journal of Heat and Fluid Flow*, Vol. 50. ISSN 0142727X. doi:10.1016/j.ijheatfluidflow.2014.08.011.

Zdravkovich, M.M., 1985. "Flow induced oscillations of two interfering circular cylinders". *Journal of Sound and Vibration*, Vol. 101. ISSN 10958568. doi:10.1016/S0022-460X(85)80068-7.

7. RESPONSIBILITY NOTICE

The authors are solely responsible for the printed material included in this paper.